

Multi-Keel Passive Prosthetic Foot Design Optimization Using the Lower Leg Trajectory Error Framework

Victor Prost¹

GEAR Laboratory,
Department of Mechanical Engineering,
Massachusetts Institute of Technology,
Cambridge, MA 02139
e-mail: vprost@mit.edu

Heidi V. Peterson

GEAR Laboratory,
Department of Mechanical Engineering,
Massachusetts Institute of Technology,
Cambridge, MA 02139
e-mail: heidip@mit.edu

Amos G. Winter, V

Associate Professor
GEAR Laboratory,
Department of Mechanical Engineering,
Massachusetts Institute of Technology,
Cambridge, MA 02139
e-mail: awinter@mit.edu

People with lower-limb amputation in low- and middle-income countries (LMICs) lack access to adequate prosthetic devices that would restore their mobility and increase their quality of life. This is largely due to the cost and durability of existing devices. Single-keel energy storage and return (ESR) prosthetic feet have recently been developed using the lower leg trajectory error (LLTE) design framework to provide improved walking benefits at an affordable cost in LMICs. The LLTE framework optimizes the stiffness and geometry of a user's prosthesis to match a target walking pattern by minimizing the LLTE value, a measure of how closely a prosthetic foot replicates a target walking pattern. However, these low-cost single-keel prostheses do not provide the required durability to fulfill International Standards Organization (ISO) testing, preventing their widespread use and adoption. Here, we developed a multi-keel foot parametric model and extended the LLTE framework to include the multi-keel architecture and durability requirements. Multi-keel designs were shown to provide 76% lower LLTE values, compared with single-keel designs while withstanding ISO fatigue and static tests, validating their durability. Given their single-part 2D extruded geometries, multi-keel feet designed with the extended LLTE framework could be cost-effectively manufactured, providing affordable and durable high-performance prostheses that improve the mobility of LMIC users.

[DOI: 10.1115/1.4055107]

Keywords: compliant mechanisms, mechanism design, prosthetics

1 Introduction

More than 80% of the lower-limb amputee population lives in low- and middle-income countries (LMICs), which represents more than 30 million people [1,2]. Due to their high cost, prosthetic devices are only accessible to about 10% of those in need [2,3], resulting in the use of inadequate devices, such as poles, crutch limbs, or dysfunctional prostheses, that require more effort and exhibit unnatural walking motions. The lack of access to adequate prostheses leaves many users subject to reduced mobility that prevents them from full employment and independent living [4–7], as many individuals with limb amputations are involved in physical and manual intensive labor [2,3].

To help restore the mobility of LMICs lower-limb amputees, affordable energy storing and return (ESR) single-keel prosthetic feet designed to store and return energy to the user have recently been developed [8–11]. ESR feet have been shown to provide improved biomechanical functionality and walking benefits to below-knee amputees, increasing the users' quality of life [12–14]. However, these single-keel ESR prostheses [8,10,11] have not been shown to provide the required durability to fulfill prosthetic foot international standards (International Standards Organization (ISO) 10328, 22675 [15,16]) that ensure the safe use of these devices over several years. The lack of durability of affordable prostheses has prevented their use and distribution in LMICs [3]. Creating affordable ESR prostheses with increased durability, while retaining the biomechanical functionality and walking benefits provided by ESR feet, could enable their widespread use

and distribution in LMICs, significantly improving the quality of life and mobility of lower-limb amputees.

The lower leg trajectory error (LLTE) framework [17] is a novel design optimization framework that streamlines the design of user-specific prostheses by quantitatively connecting the mechanical characteristics of a prosthetic foot to the gait of an amputee. The LLTE framework has been clinically validated [9,18] and used to create affordable ESR prosthetic feet to enable close to able-bodied walking patterns [8]. For a given user, a target reference walking data set, such as experimentally collected able-bodied level-ground walking data, is scaled to the person's body characteristics (mass, height, and foot length) [9]. Leg dynamics are assumed to remain in the sagittal plane. The LLTE framework then uses the constitutive model of the prosthetic foot to calculate the prosthetic side lower leg trajectory from the deformed prosthetic foot shape when subjected to the target reference walking loads [17] (ground reaction forces (GRFs) at the corresponding center of pressure (CoP) locations).

The LLTE is a single value objective metric that represents the deviation (i.e., error) between the calculated prosthetic side lower leg trajectory with that of the target reference lower leg trajectory throughout a step. The LLTE is defined as

$$\text{LLTE} = \left[\frac{1}{N} \sum_{n=1}^N \left\{ \left(\frac{x_{\text{knee},n}^{\text{model}} - x_{\text{knee},n}^{\text{ref}}}{\bar{x}_{\text{knee}}^{\text{ref}}} \right)^2 + \left(\frac{y_{\text{knee},n}^{\text{model}} - y_{\text{knee},n}^{\text{ref}}}{\bar{y}_{\text{knee}}^{\text{ref}}} \right)^2 + \left(\frac{\theta_{\text{LL},n}^{\text{model}} - \theta_{\text{LL},n}^{\text{ref}}}{\bar{\theta}_{\text{LL}}^{\text{ref}}} \right)^2 \right\} \right]^{1/2} \quad (1)$$

where the superscripts “model” and “ref” refer to values calculated by the constitutive model and values from the reference data set, respectively. N is the total number of walking frames (time instances of a step) included in the calculation, with the n indicating

¹Corresponding author.

Contributed by the Mechanisms and Robotics Committee of ASME for publication in the JOURNAL OF MECHANISMS AND ROBOTICS. Manuscript received October 14, 2021; final manuscript received July 18, 2022; published online November 8, 2022. Assoc. Editor: Just L. Herder.

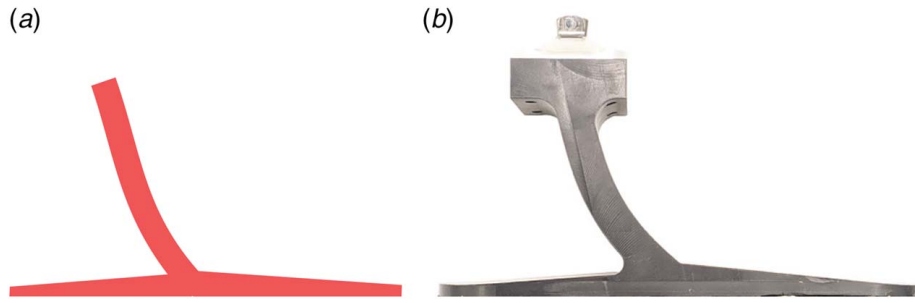


Fig. 1 Single-keel foot architecture: (a) parametric model of a single-keel foot and (b) physical embodiment of a single-keel foot

each individual frame. The knee coordinates and lower leg orientation are normalized by the mean of each reference variable across the portion of the step considered (e.g., notated by $\bar{x}_{\text{knee}}^{\text{ref}}$ for the knee horizontal coordinate). Using the LLTE value as an optimization objective metric, the prosthetic foot's mechanical characteristics (geometry and stiffness) can then be varied to minimize the resulting LLTE value [8,17], creating an LLTE-optimal foot design that enables the user to most closely replicate the target walking kinematic and kinetic data. The lower the LLTE value, the closer the replication of the target walking pattern.

Recent work has used the LLTE framework to design customized, low-cost, Nylon 6/6 ESR prostheses to replicate able-bodied level-ground walking using a single-keel single-part prosthetic foot architecture by minimizing their LLTE value [8,9] (Fig. 1). However, these LLTE-optimized single-keel prosthetic feet were designed with the optimization constraint of withstanding level-ground walking loads, not to withstand the ISO durability requirements (in terms of both static and cyclic load testing), limiting their widespread use. In addition, these single-keel prosthetic foot designs were shown to be stress-limited, meaning that further reducing the allowable peak stress values under level-ground walking loads further decreased their biomechanical performance (increased LLTE values). The LLTE design framework should be extended to include the ISO durability requirements as specific design optimization constraints, and a novel parametric foot architecture should be created to best enable the replication of the reference walking data set while satisfying the ISO durability requirements.

In this work, we designed, validated, and bench-tested a novel ESR prosthetic foot architecture, called the multi-keel architecture, to replicate level-ground walking patterns and withstand ISO durability requirements. The problem was formulated as a constrained optimization that minimized the LLTE value of multi-keel foot designs under the constraints of withstanding both walking loads and ISO durability requirements. First, the parametric multi-keel foot architecture similar to a leaf spring structure (Fig. 2) and its constitutive model were introduced to provide increased structural strength and lower LLTE values compared with the original single-keel architecture. Second, the ISO static and cyclic load testing cases were included in the LLTE framework to create multi-keel prostheses that pass the ISO durability requirements. Lastly, these multi-keel prostheses were bench-tested to validate the constitutive model and evaluated against single-keel feet to show their improved LLTE values and strength under the ISO 10328 static and cyclic tests requirements.

2 Multi-Keel Foot Architecture

2.1 High-Level Design Requirements. To ensure the safety and reliability of prosthetic feet, international standards outline a series of mechanical tests that prosthetic feet have to undergo without failure (ISO 10328 and the more recent ISO 22675 [15,16]). This study focuses on the ISO 10328 standard, which remains the most widely used standard for LMICs prostheses. The ISO 10328 standard requires prosthetic feet to withstand a

series of mechanical tests: a cyclic (2 million cycles fatigue) test that represents loading conditions typical to normal walking throughout the lifetime of the device, and singular static tests (ultimate tests) carried out to determine the load-bearing capabilities of the prosthetic foot structure under occasional severe loading conditions events [15]. These two tests require the foot to withstand (no sign of cracks, fractures, or other mechanical failures) peak loads that are respectively 1.4 and 4.6 times higher than those experienced during level-ground walking. The multi-keel foot architecture developed here should pass both the cyclic and static ISO mechanical tests. Additionally, like the prior single-keel ESR feet (Fig. 1), they should remain under a cost of 100 dollars, be mass-manufacturable, and enable able-bodied level-ground walking performance (minimized LLTE value).

2.2 Multi-Keel Architecture. The multi-keel architecture is similar to a leaf spring with a controlled gap between the two leaves of the spring (Fig. 2). The multi-keel architecture conserves the benefits of the single-keel prosthetic foot architecture [8]: it is a simple, extruded geometry that can be manufactured as a single part using low-cost materials and parameterized to allow for structural shape and size optimization.

The multi-keel prosthesis increases strength and resistance to failure, similar to leaf springs, which can be modeled by representing the foot structure as a series of Euler-Bernoulli beams. Under the Euler-Bernoulli beam model, the load capacity for a structure of similar bending stiffness scales with the number of keels, N_{keel} , as $N_{\text{keel}}^{1/3}$. A prosthetic foot with two keels could thus increase its load capacity by $2^{1/3}$, or 26%. In addition, the upper keel engaging partway through stance leads to an increased stiffness with the dorsiflexion angle of the prosthetic foot, creating a variable stiffness profile. The multi-keel variable stiffness profile is similar to the biological ankle-foot quasi-stiffness profile [19]. Independently tuning the stiffness of each keel and the size of the gap between keels can allow for a close replication of the target reference walking activity while fulfilling the ISO 10328 requirements.

2.3 Parametric Model. The multi-keel architecture was modeled as a 2D geometry using wide Bézier curves [20] (Fig. 2). A wide Bézier curve is a parametric shape defined by a series of control circles. The wide Bézier curve parameterization was chosen for its simplicity and ease of manufacturing over traditional density-based topology synthesis methodologies [21]. Using the wide Bézier curve parameterization, a cubic curve can be defined by the position of four control circle centers, reducing a potentially complex shape to a small number of design variables. The thickness of the curve is then defined as a function of the diameters of these control circles.

Three wide Bézier curves are used to describe a multi-keel foot (Fig. 2(a)). The main keel portion of the foot is modeled as a cubic wide Bézier curve, using the control circles C_1 to C_4 , followed by a linear wide Bézier curve, using the control circles C_4 and C_5 . The heel portion of the foot is described by a linear wide Bézier

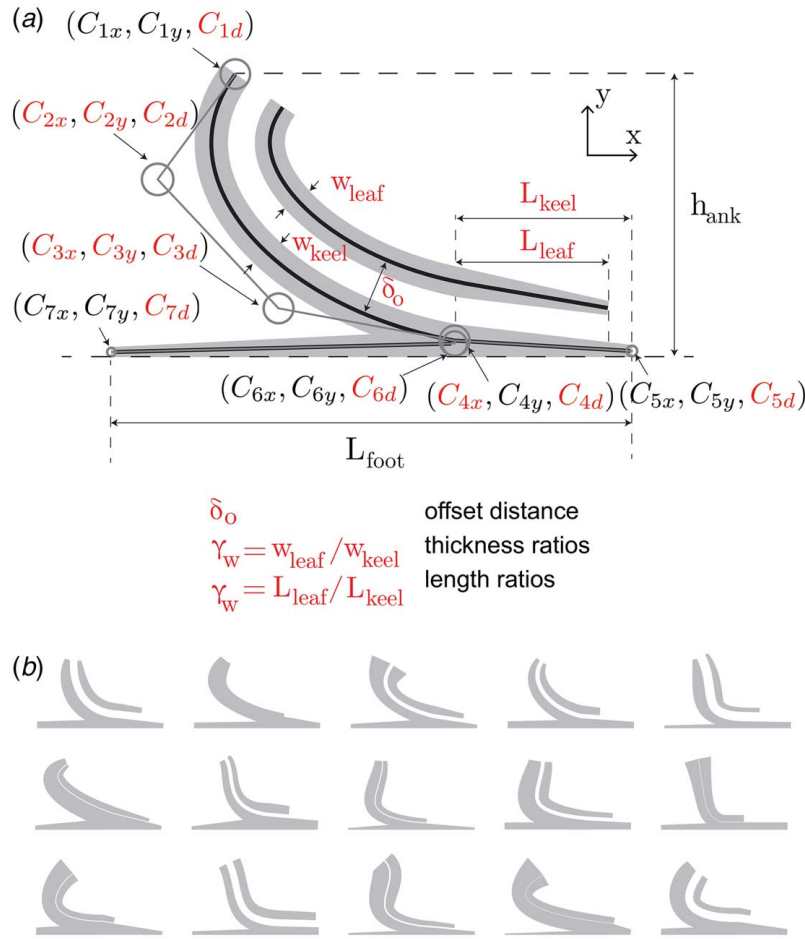


Fig. 2 Multi-keel foot architecture. (a) The multi-keel foot parametric model is defined using the Bézier curves' variables C_{ij} , geometric transformation parameters (δ_o , γ_w , γ_L), build height h_{ank} , and foot length L_{foot} . The 15 independent variables used as design parameters are shown in red. **(b)** Multi-keel prosthetic feet randomly sampled from the design space by varying each one of the 15 independent variables.

curve, using the control circles C_6 and C_7 . A radial offset geometric transformation along with a scaling transformation is then applied to the main keel wide Bézier curves to define the additional keel. The additional keel can thus be described using only three parameters: δ_o , the point-by-point radial offset distance from the main keel curve, γ_w , the ratio of the main and additional keels curve's thicknesses, and γ_L , the ratio of the main and additional keel curve's lengths.

The multi-keel architecture is entirely described by seven control circles from the wide Bézier curves and three geometric transformation parameters. Each control circle i is composed of three variables, the circle center position (C_{ix} , C_{iy}), and the circle diameter, C_{id} . Out of these 24 parametric model variables, 15 are independent design variables (Eq. (2))

$$\text{design parameters, } X = [C_{1d}, C_{2x}, C_{2y}, C_{2d}, C_{3x}, C_{3y}, C_{3d}, C_{4x}, C_{4d}, C_{5d}, C_{6d}, C_{7d}, \delta_o, \gamma_w, \gamma_L] \quad (2)$$

The remaining nine variables are set by the prosthetic user's characteristics, coupled geometric relations, and constraints. Appendix A contains these geometric relations and constraints as well as upper and lower bounds on the independent variables chosen to constrain the designs to approximately fit within the envelope of a biological foot. The multi-keel foot parameterization (Eq. (2)), used as optimization variables, enables a variety of possible prosthetic foot shapes and geometries (Fig. 2(b)).

2.4 Multi-Keel Constitutive Model. The multi-keel constitutive model describes how the prosthesis deforms and calculates the stress distribution within the prosthetic foot structure under a set of loads. The structural model was built in MATLAB (Mathworks, Natick, MA) using a custom 2D finite-element model based on frame elements [22] (Fig. 3(b)). Frame elements were chosen to represent the slender structures that compose the prosthetic foot, as these elements can undergo bending and tensile loading, capturing the mechanical behavior of the prosthesis while remaining simple with reduced computational complexity over commercially available structural analysis software. In addition, the constitutive model implemented in MATLAB with our LLTE objective function evaluation process and genetic algorithm optimization function reduced the need for external software package communication and resulted in an integrated, efficient design optimization framework.

The structural analysis was conducted in the ankle reference frame with the origin located at the prosthesis' ankle, defined at the C_1 control circle center (Fig. 2(a)). The lower leg was assumed to be a rigid body compared to the prosthetic foot [8,9]. A fixed-fixed boundary condition was applied at the prosthesis ankle: top ends of the main and additional keel were constrained in displacement and rotation. Contact between the main and additional keel was assumed to happen at the tip of the additional keel with no sliding friction, which simplified the structural analysis. Sliding friction was not included in the structural analysis to

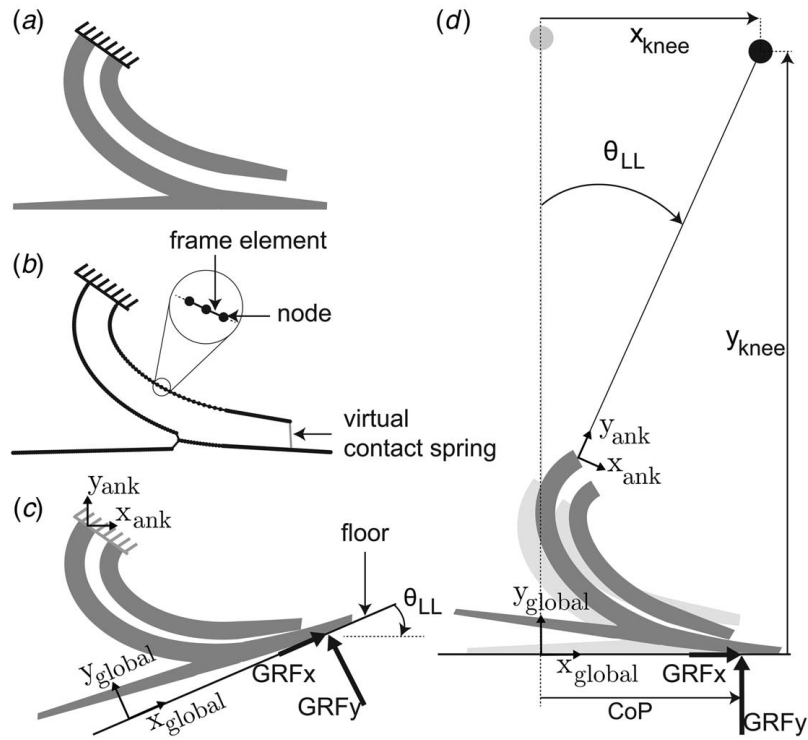


Fig. 3 Multi-keel constitutive model. (a) Multi-keel prosthetic foot model defined by the set of 15 design variables (Fig. 2(a)). (b) Finite-element model, based on frame elements, of the multi-keel foot with the virtual contact spring that enforces the nonpenetration contact condition between the two keels once contact is detected. (c) Deformed shape of the multi-keel foot in the ankle reference frame under a set of GRFs applied at a CoP. (d) Lower leg orientation and knee position in the global frame resulting from the deformation of the prosthetic foot. The undeformed shape (light gray) is overlaid with the deformed shape (dark gray) of the prosthetic foot.

reduce the source of nonlinearity in the finite-element model and significantly increase its computational efficiency. The sliding friction assumption was then tested when validating the accuracy of the chosen structural model. The contact location assumption is warranted because the GRFs are applied on the underside of the main keel and the additional keel is defined as an offset curve from the main keel.

The structural analysis starts by discretizing the prosthetic foot model into 400 frame elements, as shown in Figs. 3(a) and 3(b) (mesh size was determined through a mesh convergence analysis). Instead of applying a computational global no self-intersection boundary condition on the prosthetic foot, a local contact condition (no penetration) was applied at the tip of the additional keel where contact is assumed to happen. The local contact condition was implemented using a virtual contact spring element that connects the end frame element of the additional keel to the main keel. The virtual contact spring element's stiffness is initially set to several orders of magnitude less than the most compliant frame element's stiffness in the prosthetic foot structure. Initially, due to its low stiffness, the virtual contact springs deform without transferring loads from the main keel to the additional keel. Then, the loading on the foot (GRFs at the corresponding CoP locations for each loading case) is incrementally applied, and the nodes' locations surrounding the virtual springs are monitored for contact detection between the two keels. Once contact is detected, the additional keel is engaged by changing the stiffness of the virtual contact spring to several orders of magnitude higher than the foot frame element's stiffness. The high value of the virtual contact spring prevents penetration and transfers the normal loads from the main keel to the additional keel. The loading on the foot then proceeds until reaching the desired applied load.

Using the resulting deformed shape, the knee position and lower leg orientation are calculated in the ankle reference frame and then transformed back to the global reference frame (Figs. 3(c) and 3(d)). The lower leg orientation and the knee position for each loading case are then compared with the target reference kinematics to calculate the LLTE value for the prosthetic foot model (Eq. (1)). From the calculated knee position and the input walking loads the knee torque can also be determined. In addition, the resulting deformed prosthetic foot shape for each loading case is used to compute the stress distribution within the prosthesis and ensure that it does not exceed the prescribed allowable peak stress values.

3 Methods

3.1 LLTE Design Optimization With International Standards Organization Requirements. The loading cases for both the static and cyclic tests, described in the ISO 10328 documents, were added to the LLTE framework's structural load cases analysis compared with previous work [8,9]. The resulting stress distributions were then included in the optimization constraints with peak allowable stress values to ensure the optimized designs would satisfy the ISO requirements.

ISO 10328 loading cases consist of applying a normal load on the forefoot of the device with a plate angled 20° from horizontal, and the heel with a plate angled -15° from horizontal [15]. For both the heel and forefoot tests, the ultimate static test load levels of 3220 N for a 60 kg user and 4130 N for an 80 kg user, as well as cyclic loads (fatigue) of 970 N for a 60 kg user and 1230 N for an 80 kg user were applied to the foot structure. For each ISO loading test, a corresponding maximum allowable stress was prescribed. For the

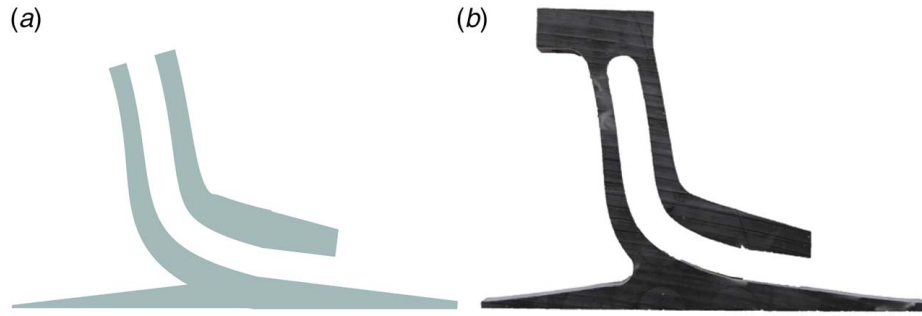


Fig. 4 Multi-keel foot architecture: (a) parametric model of a multi-keel foot and (b) physical embodiment of a multi-keel foot

ultimate static test, the maximum allowable stress level was set to the Nylon 6/6 yield stress value σ_y . For the fatigue test, the prosthetic foot had to undergo 2 million cycles according to ISO 10328. Therefore, the stress level within the foot had to remain under the million cycles fatigue stress σ_{Mf} rating for Nylon 6/6 [23], which was set as the maximum allowable stress for the fatigue loading case. For the walking load conditions, the maximum stress level was prescribed to remain below the material's yield strength with a prescribed safety factor of 1.75 similar to previous work conducted using the LLTE framework [8,9] (safety factor being defined as the ratio between the material yield stress and the allowable peak stress in the structure under walking load conditions).

The LLTE framework optimization problem solved to design the foot was the following:

$$\begin{aligned} \min_X \quad & \text{LLTE}(X) \\ \text{s.t.} \quad & \text{self-intersecting} \leq 0 \\ & \sigma_{\max}^i - \sigma_{\text{allow}}^i \leq 0 \end{aligned} \quad (3)$$

where X corresponds to the design parameters (Eq. (2)) that define the prosthetic foot model. The self-intersecting optimization constraints are geometric conditions that prevent the structure from self-intersecting as outlined in previous work [8]. The stress optimization constraints ensure that the maximum stress level in the structure remains below the allowable peak stress value for each loading scenario. The index i for the allowable peak stress value differentiates between the ISO ultimate loading tests, the ISO fatigue tests, and the target walking pattern loading conditions.

The optimization was implemented in MATLAB and solved using the built-in genetic algorithm function [24] similar to Olesnavage et al. [8]. The LLTE value (objective function) was implemented as a custom script along with the prosthetic foot model described in Sec. 2.4. To increase the likelihood of returning a global optimum, the genetic algorithm optimization was repeated five times with different initialization parameters and the resulting designs were checked to be nearly identical.

3.2 Prosthetic Foot Design Using the LLTE Framework.

Nylon 6/6 was chosen as the material for the prosthetic feet due to its low cost, high strain-energy density ($u \approx 2.4 \cdot 10^3 \text{ J/kg}$) and strength (ultimate flexural stress of 124 MPa). The experimentally measured material characteristics of Nylon 6/6 were incorporated in the multi-keel constitutive model with a tensile modulus $E = 2.51 \text{ GPa}$, tensile yield stress $\sigma_y = 82.7 \text{ MPa}$, flexural modulus $E_f = 3.15 \text{ GPa}$, flexural yield stress $\sigma_{yf} = 92.0 \text{ MPa}$, and density $\rho = 1130 \text{ kg/m}^3$.

Four prosthetic feet, two for both foot architectures (single and multi-keel), were optimized for able-bodied level-ground walking (using able-bodied reference data from D.A Winter [25]) using the extended LLTE framework that includes the ISO loading case

requirements and the corresponding allowable peak stress values in the optimization (Sec. 3.1). The two sets of two prosthetic feet were designed for users with a height of 1.70 m, foot length of 0.25 m, foot width of 0.06 m, ankle height of 0.11 m, and body mass of, respectively, 60 kg and 80 kg. These two body masses were chosen for both foot architecture to reflect the male and female average user body characteristics in LMICs [26]. The target level-ground able-bodied walking data were scaled to the user's body characteristics. The GRFs were scaled by the user body mass, the CoP locations by the user foot length, and the lower leg trajectory by the user lower leg length [17]. The stiffness and geometry of the prosthetic foot architectures were tuned to minimize the LLTE value for level-ground walking while satisfying the maximum allowable peak stress values from the ISO requirements and level-ground walking loading conditions. The LLTE value of each of the four resulting prosthetic foot was recorded before being tested for fatigue loading in numerical simulation and for static ultimate strength on the mechanical apparatus described in Sec. 3.5.

3.3 Prototype Manufacturing. The LLTE-optimized prosthetic feet were manually post-processed to include a surface mount to match the prosthetic leg mounting system. The prosthesis ankle and additional keel in the constitutive model are rigidly fixed to the rest of the prosthesis. To best replicate the fixed end condition of both keels without modifying the mechanical characteristics of the prosthesis, material was added to the ankle to couple the keels and create the rigid fixture with a horizontal surface to which a male pyramid adapter, the standard attachment for prosthetic components, could be mounted.

The resulting foot designs were machined, using a waterjet and milling machine, out of a cast block of Nylon 6/6. The series of prototypes (Fig. 4) were manufactured with reduced widths of 16 mm instead of the designed full width of 60 mm. The reduced width enabled faster iteration and testing while maintaining high fidelity compared with full-width devices. The correlation between the full and reduced width device can be done by linearly scaling the applied load to the prototype's width during mechanical testing, as the stiffness of the compliant structure is determined by the beam bending and tensile stiffnesses. The reduced-width prototypes were subjected to mechanical tests to validate the multi-keel prosthetic foot model (Sec. 3.4) as well as the ISO static ultimate tests (Sec. 3.5) to test their durability.

3.4 Multi-Keel Constitutive Model Validation Using Mechanical Testing.

To validate the multi-keel constitutive model, static mechanical tests were conducted on the set of multi-keel prototype prosthetic feet (Sec. 3.2) using an Instron load testing machine (Instron Inc., Norwood, MA). The measured displacements of the prototype feet in response to loading were compared with the constitutive model results.

The experimental setup consisted of a jig constraining the test foot while the Instron applied loads similar to the load experienced by a target user when walking on level ground at self-selected speed ($F \approx 700$ N). Loads were scaled to $F \approx 186$ N to match the reduced-width prototypes. Loads were applied at two locations along the foot, $CoP_{keel} = 130 \pm 0.1$ mm and $CoP_{heel} = -30 \pm 0.1$ mm, measured from the prosthesis ankle (Fig. 5). The foot was loaded at a constant rate of 300 mm/min. The vertical load ($F_{instron}$) and displacement ($x_{instron}$) of the Instron head were recorded at a rate of 10 Hz (Fig. 5(a)). The Instron load cell is resistant to off-axis loading errors, with a rated maximum force measurement error of 6.4%. The Instron head displacement was measured with a rated error of ± 0.1 mm. The custom jig fixed on the Instron machine is composed of a linear stage on which an aluminum rod is mounted on a set of roller bearings to minimize friction. The rod ensures that the applied load remains normal to the foot and can be applied at specific CoPs along the foot (Fig. 5).

The experimental setup's loading conditions (heel and keel loading) were replicated using the multi-keel constitutive model for each multi-keel prototype test foot (Sec. 3.2). The modeled load–displacement data were then compared with the measured Instron values to validate the accuracy of the multi-keel constitutive model. In addition, the energy storage and return efficiency of the prototype feet were calculated as the ratio of the stored and returned elastic energy using the loading and unloading load–displacement data, respectively [27]. A numerical validation of the accuracy of the 2D finite-element model implemented in MATLAB with a commercially available software was also conducted and included in Appendix B.

3.5 International Standards Organization 10328 Static Case Mechanical Testing. To ensure that the designed single- and multi-keel feet (Secs. 3.1–3.2) withstand the ISO 10328 ultimate static tests without failure (Sec. 2.1), the ultimate static mechanical heel and forefoot strength tests were conducted on the prototype prosthetic feet using an Instron load testing machine. The ISO 10328 static tests use a different experimental setup from Sec. 3.4 which consists of another jig that constrains the test foot (Fig. 6) at a prescribed angle while the Instron applies the ISO ultimate static tests loads ($F_{ult} = 3220$ N and 4130 N for the 60 kg and 80 kg devices, respectively, and scaled to 860 N and 1100 N to match the prototypes' reduced widths). The prototype feet were fixed at the required angle (20° for the forefoot and -15° for the heel) and loaded on a horizontal plate with a Teflon (PTFE) sheet to minimize shear loading on the devices. The foot was loaded at a constant rate of 100 N/s, matching the ISO testing protocol. The vertical load ($F_{instron}$) and displacement ($x_{instron}$) of the Instron head were recorded at a rate of 25 Hz. In the ISO 10328 experimental setup described here, the Instron rated maximum force measurement error was $\pm 2.5\%$ and head

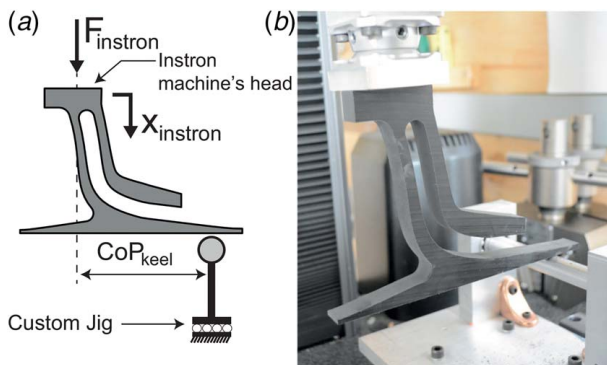


Fig. 5 Mechanical tests experimental setup: (a) schematic of the experimental setup and (b) photograph of a prototype prosthetic foot being loaded on the Instron machine

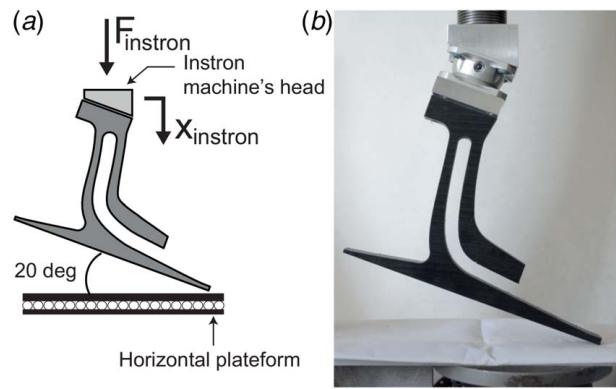


Fig. 6 ISO ultimate static tests experimental setup: (a) schematic of the experimental setup and (b) photograph of a prototype prosthetic foot being loaded on the Instron machine

displacement measurement error was ± 0.1 mm. The ultimate static tests were repeated twice for each prototype to check for any plastic deformation within the prosthetic feet that would indicate mechanical failure.





3.6 Numerical Fatigue Analysis. To test the ability of the prosthetic feet to withstand the ISO fatigue test requirement, a numerical simulation fatigue tool was used to replicate the ISO 10328 fatigue test (Sec. 2.1). The prosthetic foot models were constructed in SOLIDWORKS and then imported into ANSYS WORKBENCH (Student 2020 R1 version), a standard fatigue simulation tool [28]. The simulated test consisted of heel and forefoot platforms angled at -15° and 20° , respectively, applying specified forces in an alternating and sinusoidal pattern. After inputting the stress life characteristic (S–N curve) for Nylon 6/6 [23], the Ansys fatigue tool was used to predict the fatigue life of the foot under the combined loading scenario. The available S–N curve for Nylon 6/6 provided information up to 1 million cycles, the fatigue life for which the feet were simulated. The completion of 1 million cycles of the ISO 10328 test by a prosthetic foot would provide sufficient evidence of durability, since the maximum allowable stress for the fatigue test could always be further reduced to enable 2 million cycles (reduction of about 5% in the allowable stress from 1 to 2 million cycles, as S–N curves are log scale curves). A preliminary experimental fatigue test, detailed in Appendix C, was conducted with a single-keel prosthetic foot prototype manufactured out of Nylon 6/6 to further warrant the use the ANSYS fatigue simulation tool.

4 Results

4.1 Prosthetic Feet Optimized for LLTE Value and International Standards Organization Requirements. Table 1 includes the LLTE values of the resulting optimal designs for 60 and 80 kg users for level-ground walking for both foot architectures. Single-keel prosthetic feet achieved LLTE values of 0.416 and 0.832 for the 60 and 80 kg users, respectively. Multi-keel prosthetic feet achieved LLTE values of 0.127 and 0.145, respectively, which are 69% and 82% lower than those of the single-keel designs. In other words, multi-keel prosthetic feet designed for ISO strength requirements could enable a closer replication of the target able-bodied level-ground walking motion when compared with single-keel prosthetic feet. However, the improvement in LLTE values from the multi-keel designs come at an increased prosthesis mass of 0.06 and 0.09 kg, respectively. The design variables describing each foot design can be found in Appendix D.

The optimization constraints on peak stress value were active for both single-keel feet designs for the ISO 10328 cyclic test conditions. For the 80 kg single-keel design, the optimization constraint

Table 1 Prosthetic foot designs optimized using the LLTE framework to replicate level-ground walking and withstand the ISO strength requirements

	Single-keel	Single-keel	Multi-keel	Multi-keel
				
Body mass (kg)	60	80	60	80
Foot mass (kg)	0.29	0.31	0.35	0.40
LLTE	0.416	0.832	0.127	0.145
Predicted fatigue life	>1M cycles	>1M cycles	>1M cycles	>1M cycles

Notes: The four foot design models, masses, LLTE values, and predicted fatigue lives, as well as the target users' body masses are shown here. The allowable maximum stress for each loading scenario (walking loads or ISO loading cases) is described in Sec. 3.1.

on peak stress value was also active for the ISO 10328 ultimate static test conditions. On the contrary, the optimization constraints on peak stress values were not active for multi-keel feet. The multi-keel foot designs' peak stress values were between 82% and 93% of the allowable stress values (Sec. 3.1). While multi-keel designs result in improved walking performance, single-keel prostheses can still be designed for the ISO strength requirements at the detriment of reduced LLTE walking performance. A sensitivity study that further investigates the impact of strength requirements on the LLTE walking performance of prosthetic feet can be found in Appendix E.

4.2 Mechanical Testing Validation of the Multi-Keel Constitutive Model. The multi-keel constitutive model accurately represented the measured deformations from the foot prototypes (Fig. 7), warranting its use in the LLTE framework to evaluate the LLTE value of multi-keel feet. Across both prosthetic foot prototypes and the two loading cases (heel and keel), the displacements of the prostheses were predicted with a maximum error of 2.1 mm over deformations up to 34.3 mm. The average error across all the conditions over the load–displacement curve was 0.6 ± 0.3 mm or $5.6 \pm 3.9\%$.

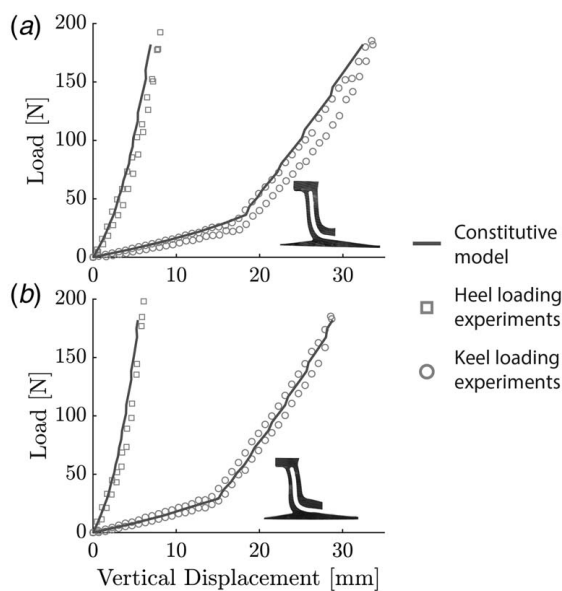


Fig. 7 Load–displacement curves for the two multi-keel prosthetic foot prototypes (a, b) measured with the Instron machine and compared with the constitutive model results. The prototypes were tested at the heel ($\text{CoP}_{\text{heel}} = -30 \pm 0.1$ mm) and at the keel ($\text{CoP}_{\text{keel}} = 130 \pm 0.1$ mm). Prototype a corresponds to a 60 kg user, and prototype b to an 80 kg user.

The energy storage and return efficiency of these prototypes were on average $92.4 \pm 4.4\%$ (Fig. 7). The deformation of the prototypes was not purely elastic due to viscoelasticity in the material and friction losses at the contact between the two keels. Using the constitutive model prediction of the contact forces F_c , the sliding motion between the two keels δ_s , and a sliding contact friction coefficient for Nylon 6/6 of $\mu_d = 0.26$, the energy loss due to contact friction, W_{friction} , can be estimated to be on average $3.6 \pm 1.2\%$ with $W_{\text{friction}} \approx \int \mu_d F_c d\delta_s$. These small efficiency losses do not significantly impact the deformation predictions of the purely elastic multi-keel constitutive model.

4.3 International Standards Organization Benchtop Test Validation of Ultimate Strength Test Requirements. All four prosthetic foot prototypes withstood the ultimate static tests on the Instron machine for both the heel and forefoot loading conditions. The deformed shapes of a prosthetic foot prototype at four loading levels during the ultimate static tests are shown in Fig. 8. None of the prosthetic feet showed any signs of cracks, fractures, or mechanical failures. For each foot prototype, the second run of the ultimate static test resulted in a maximum difference of 0.1 mm in the measured peak displacements for the forefoot loading case and 0.3 mm for the heel loading case. The fact that these in-between trial differences are within the load and displacement measurement accuracy of the Instron machine suggests that the foot prototypes underwent minimal or no plastic deformation. The measured load–displacement curves of the ultimate static tests for the four prosthetic foot prototypes are included in Appendix F.

4.4 Prosthetic Feet Achieve Target Fatigue Life. None of the prosthetic foot models broke within the simulation of 1 million cycles (Table 1), the maximum number of cycles on the Nylon 6/6 S–N curve used in the fatigue test simulation. The resistance to 1 million cyclic testing suggests that with a suitable safety factor (or choice of σ_{Mf} , the maximum allowed stress under cyclic tests, defined in Sec. 3.1), the LLTE framework could be used to design feet that satisfy the ISO 10328 cyclic fatigue requirement of 2 million cycles.

5 Discussion

This study demonstrates that the LLTE design framework can be extended to include additional prosthesis strength requirements and diverse foot architectures. The multi-keel architecture and parameterization (Figs. 2–4) were integrated in the LLTE framework and resulted in designs with minimized LLTE values that meet the ISO 10328 requirements. These results reinforce the use of the LLTE framework as a prosthetic foot design tool to optimize foot architectures as long as an accurate constitutive model of these architectures can be built. In this work, a finite-element model (Fig. 3) accurately modeled the constitutive behavior of the

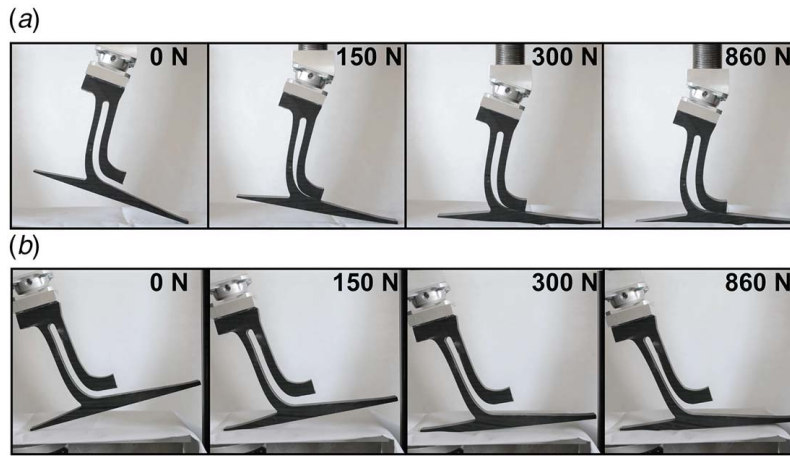


Fig. 8 Multi-keel prosthetic foot tested under the ISO ultimate static loading cases in the Instron machine corresponds (a) to the forefoot loading and (b) to the heel loading scenario. The prosthetic foot shown here corresponds to the 60 kg user design.

multi-keel foot architecture with an average error of 5.7% (Fig. 7) compared with measured displacements. The finite-element model is critical to the optimization process, as it evaluates the LLTE value and peak stress for each multi-keel design. There is a tradeoff between the complexity of the parametric model, which determines the accuracy of the constitutive model, and the ability of the LLTE optimization framework to converge to an optimal solution in a reasonable amount of time. The prosthetic foot parametric model uses 15 design variables and a low-dimensional structural model that conducts the structural analysis and evaluates the LLTE of a multi-keel foot design in an average of 0.292 s, which enables the optimization of a prosthetic foot in an average of 2 h.

Affordable single-part Nylon 6/6 prosthetic feet were designed using the LLTE framework to enable the replication of level-ground walking while withstanding the ISO 10328 strength requirements. Both single-keel and multi-keel feet were shown to withstand the ultimate static tests (Fig. 8) and one million cycles of the simulated fatigue tests (Sec. 4.4). Compared with the single-keel foot structure, the multi-keel architecture resulted in foot designs with increased performance, demonstrated by a lower LLTE value, increased strength and limited added mass [29] (Fig. 10). Multi-keel prosthetic foot designs that withstood the ISO 10328 strength requirements achieved an average of 76% lower LLTE values compared with single-keel designs (Table 1). In addition, the LLTE values of the multi-keel prostheses were similar when designed for users of different body mass whereas the LLTE values of single-keel prostheses increased when designed for increased user body mass (60–80 kg). The increase in LLTE value for varying user body mass and the optimization constraints on peak allowable stress being active for the single-keel LLTE-optimal designs further illustrate that these designs are stress-limited [8,9] (Table 1). This effect is also described in the strength sensitivity study described in Appendix E (Fig. 10). In order to prevent mechanical failure, the designs are made stronger at the detriment of their walking performance. On the contrary, the multi-keel prostheses do not seem to be stress-limited, since the optimal designs maintained a similar LLTE value when designed for users with increased mass. The resilience for users with high body mass is a major advantage with the worldwide increase in body weight [30] and the increase in strength requirements from international standards. These results suggest that multi-keel feet can enable a closer replication of level-ground walking activity and increased structural strength compared with the single-keel feet, which could result in improved durability and mobility for prosthesis users.

The work presented here is mainly focused on the mechanics of level-ground walking in 2D, within the sagittal plane, where more

than 90% of the ankle work is performed [31]. Expanding the analysis to 3D would further increase the functionality of LLTE-designed prosthetic feet. However, the expansion to 3D would exponentially increase the complexity of the structural constitutive model as well as the optimization process in its current form. Nonetheless, to account for some out-of-plane functionalities, prosthetic foot features or design changes can be added to the LLTE framework without affecting the prosthetic foot's sagittal plane mechanical characteristics. These additions may include integrating split keels, toes, heels, or a torsional joint [32] for uneven terrain, or reducing the width at the ankle while maintaining the same bending stiffness to allow for increased side to side (coronal plane) compliance. This study focused on the level-ground walking pattern only and could be extended to include additional walking activities along with considerations on the variability in the human walking pattern by implementing robust and multi-objective optimization techniques.

Previous clinical studies have shown the effectiveness of prosthetic foot prototypes designed using the LLTE [9,18]. Similar clinical testing with transtibial amputees, field pilots and mechanical fatigue testing are needed to further validate the multi-keel foot architecture and the ability of the LLTE design framework to create prostheses customized for a specific user's characteristics and target walking activity while withstanding the ISO strength requirements.

6 Conclusions

Single-part ESR prosthetic feet made of low-cost plastic, Nylon 6/6, were designed using an extended LLTE framework to enable the replication of level-ground walking while withstanding the ISO 10328 strength requirements. A novel multi-keel foot parametric model based on wide Bézier curves and a constitutive model based on finite-frame elements were introduced to enable increased walking performance and structural strength compared with single-keel prosthetic foot designs. Multi-keel feet optimized to replicate level-ground walking and withstand the ISO 10328 strength requirements resulted in LLTE values 76% lower than those of single-keel designs. Prototype multi-keel designs were built and tested on an Instron material testing machine to demonstrate the structural finite-element model used in the LLTE design framework. The measured displacements were predicted with an accuracy of 0.6 ± 0.3 mm or $5.6 \pm 3.9\%$ across all prototypes. Mechanical ultimate static tests following the ISO 10328 standard were conducted on the multi-keel and single-keel prototypes, resulting in no mechanical failure and validating the ability of the extended LLTE framework to

design devices that can withstand the ISO 10328 strength requirements.

The simulation results and initial mechanical testing have validated an extended LLTE design framework that includes the ISO 10328 strength requirements and a multi-keel constitutive model, warranting clinical studies and field trials with below-knee amputees to further demonstrate the utility of the design methodology and these multi-keel prostheses.

Acknowledgment

The work presented here was funded by the Office of the Assistant Secretary of Defense for Health Affairs, through the Peer Reviewed Orthopedic Research Program under Award No. W81XWH-17-1-0427. Opinions, interpretations, conclusions, and recommendations are those of the author and are not necessarily endorsed by the Department of Defense. The authors would like to thank Josephine V. Carstensen, Susan Amrose, Charlotte Folinus, Nina T. Petelina, and Grace Connors at MIT for their support.

Conflict of Interest

There are no conflicts of interest.

Data Availability Statement

The datasets generated and supporting the findings of this article are obtainable from the corresponding author upon reasonable request.

Appendix A: Multi-Keel Parametric Model Constraints, and Upper and Lower Bounds

The multi-keel architecture is entirely described by the seven control circles from the wide Bézier curves and the three geometric transformation parameters. Out of these 24 parametric model variables, 15 are independent design variables (Eq. (2)).

The remaining nine variables are set by the prosthetic user's characteristics, coupled geometric relations, and constraints. The center position of control circle C_1 is defined as our reference origin, so $C_{1x}=0$ and $C_{1y}=0$. The height of the prosthetic foot h_{ank} is prescribed by the user's stump length, and the foot is constrained to be flat on the ground, which leads to the y -positions of the control circles C_4 to C_7 to be constrained. The y -position of each one of these four control circles, indexed as j , can be calculated as $C_{jy} = -h_{\text{ank}} + C_{jd}/2$. The length of the user's foot defines the horizontal locations of the control circles 5 and 7, C_{5x} and C_{7x} . The heel and the main keel curves are connected together which leads to $C_{4x} = C_{6x}$. In addition, geometric constraints similar to those in our previous work [8] were set on both keel shapes to prevent self-intersections which would result in nonphysical structures.

Upper and lower bounds (Eqs. (A1), (A2)) were imposed on each of the 15 independent variables to constrain the shape and size of the structure to approximately fit within the envelope of a biological foot. All control circle position and diameter are shown in m

$$\begin{aligned} \text{lowerbounds} = & [0.005, -0.070, -0.060, 0.005, -0.070, \\ & -0.080, 0.005, 0.010, 0.005, 0.001, \\ & 0.005, 0.001, 0.001, 0.05, 0.20] \end{aligned} \quad (\text{A1})$$

$$\begin{aligned} \text{upperbounds} = & [0.040, 0.020, 0, 0.040, 0.020, \\ & 0, 0.030, 0.130, 0.030, 0.030, \\ & 0.025, 0.025, 0.02, 1.25, 0.95] \end{aligned} \quad (\text{A2})$$

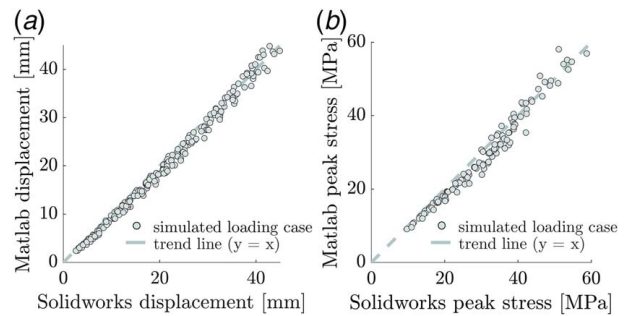


Fig. 9 Displacements at the CoP (a) and maximum von Mises stress (b) of prosthetic foot models under load; calculated with SOLIDWORKS and the MATLAB constitutive model (FEA)

Appendix B: Numerical Validation of the MATLAB-Based Constitutive Model Using SOLIDWORKS

The SOLIDWORKS structural analysis software was used to further validate the multi-keel constitutive model displacement and maximum stress predictions. Four multi-keel prosthetic foot models were constructed in SOLIDWORKS and large displacement nonlinear static load analyses were performed with vertical loads applied at varying centers of pressure (CoPs) along the foot. The prosthetic foot models were constructed for a target user mass of 60 kg, height of 1.70 m, foot length of 0.25 m, ankle height of 0.11 m, and lower leg length of 0.50 m.

For each foot model, seven vertical ground reaction forces, GRF_y , ranging from 200 N to 500 N with 50 N increments were applied at six CoPs ranging from 0.05 m to 0.15 m with 0.02 m increments. A contact set was defined between the two keels to prevent penetration with a friction coefficient between the two Nylon 6/6 keels of $\mu_d=0.26$. A triangular mesh size of 0.6 mm was chosen through a mesh convergence analysis to provide high prediction accuracy. The large displacement formulation was chosen since the prosthetic foot structure behaves as a compliant mechanism. In addition, a force control Newton–Raphson method was selected for the iteration technique due to the internal contact during the deformation of the prosthetic foot model.





For each one of these 42 loading cases, the vertical displacement at the CoP and the maximum von Mises stress within the four-foot models were recorded. These loading cases were replicated using the MATLAB multi-keel constitutive model for each foot model. The load–displacement data and maximum von Mises stress were then compared with SOLIDWORKS values to ensure the accuracy of the multi-keel constitutive model.

The multi-keel constitutive model accurately represented the simulated deformations and stress levels. Across all four prosthetic foot models and the 42 loading cases, the displacements of the prostheses were predicted with a maximum error of 3.7 mm at deformations of 42.5 mm compared with the SOLIDWORKS results (Fig. 9). The average error across all the conditions over the load–displacement curve was 1.2 ± 0.8 mm or $6.7 \pm 5.1\%$. Similarly, the maximum stress within the foot models was predicted with an average error of 2.1 ± 1.3 MPa or $7.4 \pm 6.2\%$. Each loading case took an average of 3 min 25 s to process using SOLIDWORKS and 0.172 s using the MATLAB model.

Appendix C: Prosthetic Foot Experimental Fatigue Test

An exploratory experimental fatigue test was conducted as a preliminary validation of the ANSYS fatigue simulation tool. The single-keel prosthetic foot designed by Olesnavage et al. [8] and manufactured out of Nylon 6/6 was physically tested on an ISO 10328 cyclic testing machine. During the test, the prototype broke at the heel after 58,000 cycles. The ANSYS simulation tool

Table 2 Design parameters of the ISO compliant prototype foot designs created using the extended LLTE framework and shown in Table 1

				
Body mass (kg)	60	80	60	80
Lower leg length (m)	0.50	0.50	0.50	0.50
Foot length (m)	0.25	0.25	0.25	0.25
Ankle height (m)	0.11	0.11	0.11	0.11
Design variables	[0.012, 0.015, -0.050, 0.010, 0.014, -0.079, 0.005, 0.044, 0.019, 0.004, 0.015, 0.002]	[0.016, -0.019, -0.040, 0.020, -0.008, -0.066, 0.018, 0.014, 0.019, 0.004, 0.015, 0.005]	[0.010, 0.011, -0.032, 0.005, 0.000, -0.091, 0.008, 0.039, 0.016, 0.003, 0.015, 0.002, 0.008, 1.250, 0.201]	[0.007, 0.009, -0.059, 0.006, 0.008, -0.094, 0.016, 0.044, 0.016, 0.004, 0.019, 0.002, 0.010, 1.250, 0.346]

Note: The design variables are the independent variable values for the single or multi-keel parametric model that defines their geometry and size.

predicted that the model would break at a similar location at the heel after 36,000 cycles. Although additional experimental testing is required, this initial result warranted the use of this fatigue simulation tool to predict the breakpoint and estimate the fatigue life of foot models.

Appendix D: Prototype Feet Design Parameters

The list of parameters used in the LLTE framework to design each prototype foot as well as the parametric design variables describing their geometry and size are shown in Table 2.

Appendix E: Single and Multi-Keel LLTE-Optimal Foot Sensitivity Relative to the Optimization Constraints on Allowable Peak Stress Values

To compare the tradeoff between walking performance (LLTE value) and increased strength (reduced allowable peak stress values in the optimization constraints, leading to increased safety factors) between the single and multi-keel architecture, a numerical sensitivity investigation was carried out to systematically compare the achieved LLTE-optimal values between single and multi-keel

feet for varying level-ground walking loads safety factor values (Sec. 3.1). The same representative prosthesis user from Sec. 3.2 was used in the numerical sensitivity analysis (body mass of 60 kg and height of 1.70 m). Nylon 6/6 was used as the prosthesis material along with able-bodied level-ground walking as the target reference data [25]. Feet were optimized for minimum LLTE with varying safety factor values in the optimization constraints. The safety factor was varied from 1.3 to 3 with increments of 0.1, meaning that the peak stress in the resulting optimal foot design across all the loading cases from the reference walking data was constrained to be 1.3–3 times lower than the material’s yield stress. The range of safety factors for level-ground walking loads was chosen to represent the peak loads users might apply on the prosthesis under different walking activities [33]. The LLTE values of the resulting optimal prosthetic feet were recorded and compared between the two architectures.

Multi-keel designs achieved reduced LLTE values when compared with single-keel designs with similar safety factor values. Using a multi-keel instead of a single-keel LLTE-optimal design for level-ground walking reduced the LLTE value by an average of 55% at similar safety factor values and a max of 76% (Fig. 10). For a chosen safety factor of 2, the LLTE-optimal multi-keel design LLTE value was 0.115, 73% lower than 0.428, the LLTE value of the corresponding single-keel design.

Using a multi-keel instead of a single-keel foot with similar LLTE values (walking performance) for level-ground walking resulted in an average safety factor increase of 24% (Fig. 10). The single-keel LLTE-optimal foot that achieved an LLTE value of 0.338 had a safety factor of about 1.8, while the corresponding multi-keel foot with a similar LLTE value had a safety factor of 2.3, 28% higher than the single-keel foot with a similar LLTE value. The average mass of single and multi-keel designs was respectively 0.29 ± 0.02 kg and 0.38 ± 0.02 kg. The increased safety factor values from the multi-keel designs, achieved without trading-off performance (no LLTE value change), warrant its consideration as a more durable ESR alternative to single-keel designs.

For both foot architectures, increasing the safety factor seems to increase the LLTE-optimal foot’s LLTE value (Fig. 10). In addition, the results suggest that when the safety factor decreases under a given threshold value, the LLTE value achieved by the LLTE-optimal feet starts to plateau. The plateau region suggests that for a certain choice of safety factors, designs are not stress-limited, and the walking performance of the prostheses is no longer affected by the safety factor constraint. For multi-keel feet, the plateau LLTE value is about 0.096 with a safety factor threshold of approximately 2.1. For single-keel feet, the plateau LLTE value is about 0.305 with a safety factor threshold of approximately 1.6. Multi-keel feet achieved lower LLTE values and had a wider plateau region when compared with single-keel designs.

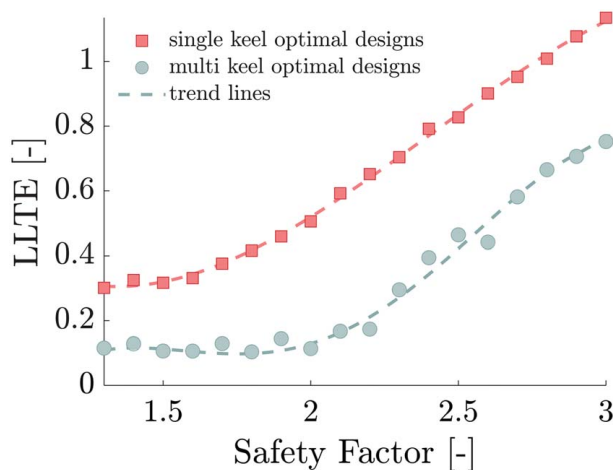


Fig. 10 LLTE values of single-keel (square markers) and multi-keel (round markers) feet optimized for level-ground walking at a comfortable speed for safety factors ranging from 1.3 to 3. The dashed lines are the fourth-order polynomial fit representing the trend between optimal LLTE value and safety factor constraint for both foot architectures.

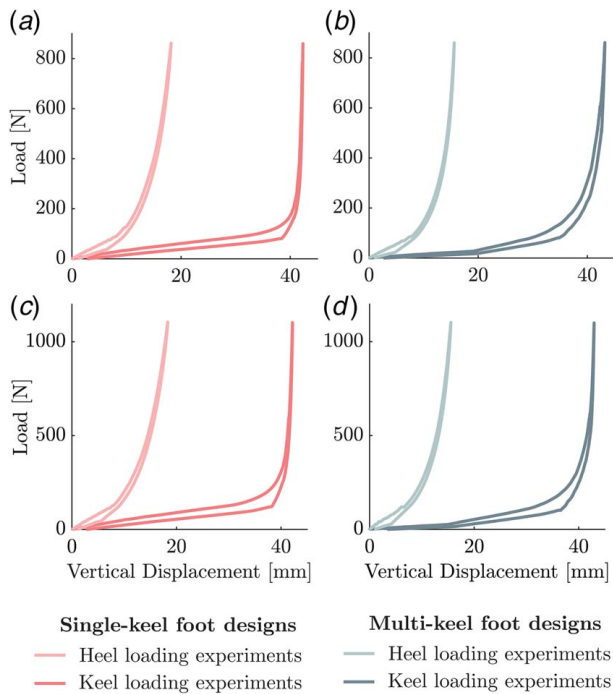


Fig. 11 Load–displacement curves of the four ISO compliant prosthetic foot prototypes (a)–(d) tested for the ISO ultimate static strength on the Instron machine. The prototypes were loaded on the heel at a -15° angle and on the keel at a 20° angle. Prototypes a and b correspond to a 60 kg user (loaded to 860 N), and prototypes c and d to an 80 kg user (loaded to 1100 N). The red solid lines correspond to the single-keel feet and the teal solid lines to the multi-keel feet.

Appendix F: International Standards Organization Benchtop Tests

The load–displacement curves of the four prototype prosthetic feet (two single-keel and two multi-keel) designed using the extended LLTE framework to withstand the ISO 10328 strength requirements are shown in Fig. 11. All prosthetic feet enter a self-locking position where they resist the load in compression instead of bending as seen in a major load increase with minimal vertical displacement on all four load–displacement curves (Fig. 11). The self-locking position can be seen in the last two frames of the keel ISO ultimate test loading photographs in Fig. 8(a), where the main keel is flat on the ground and the loads are resisted in compression rather than bending.

References

- [1] Ziegler-Graham, K., MacKenzie, E. E. J., Ephraim, P. L. P., Trivison, T. G., and Brookmeyer, R., 2008, “Estimating the Prevalence of Limb Loss in the United States: 2005 to 2050,” *Arch. Phys. Med. Rehabil.*, **89**(3), pp. 422–9.
- [2] World Health Organisation, 2011, World Report on Disability, Technical Report, World Health Organisation.
- [3] Laferrier, J. Z., Groff, A., Hale, S., and Sprunger, N. A., 2018, “A Review of Commonly Used Prosthetic Feet for Developing Countries: A Call for Research and Development,” *J. Nov. Physiother.*, **8**(1), pp. 1–10.
- [4] Norvell, D. C., Czerniecki, J. M., Reiber, G. E., Maynard, C., Pecoraro, J. A., and Weiss, N. S., 2005, “The Prevalence of Knee Pain and Symptomatic Knee Osteoarthritis Among Veteran Traumatic Amputees and Nonamputees,” *Arch. Phys. Med. Rehabil.*, **86**(3), pp. 487–493.
- [5] Gailey, R., Allen, K., Castles, J., Kucharik, J., and Roeder, M., 2008, “Review of Secondary Physical Conditions Associated With Lower-Limb Amputation and Long-Term Prosthesis Use,” *J. Rehabil. Res. Dev.*, **45**(1), pp. 15–30.
- [6] Zidarov, D., Swaine, B., and Gauthier-Gagnon, C., 2009, “Quality of Life of Persons With Lower-Limb Amputation During Rehabilitation and at 3-Month Follow-Up,” *Arch. Phys. Med. Rehabil.*, **90**(4), pp. 634–645.

- [7] Waters, R. L., and Mulroy, S., 1999, “The Energy Expenditure of Normal and Pathologic Gait,” *Gait Posture*, **9**(3), pp. 207–231.
- [8] Olesnavage, K. M., Prost, V., Johnson, W. B., and Amos Winter, V. G., 2018, “Passive Prosthetic Foot Shape and Size Optimization Using Lower Leg Trajectory Error,” *ASME J. Mech. Des.*, **140**(10), p. 102302.
- [9] Prost, V., Johnson, W. B., Kent, J. A., Major, M. J., and Winter, A. G., 2022, “Biomechanical Evaluation Over Level Ground Walking of User-Specific Prosthetic Feet Designed Using the Lower Leg Trajectory Error Framework,” *Sci. Rep.*, **12**(1), pp. 1–15.
- [10] Lopez-Avina, G. I., Barocio, E., and Huegel, J. C., 2017, “Pseudo Fatigue Test of Passive Energy-Returning Prosthetic Foot,” 2017 IEEE Global Humanitarian Technology Conference (GHTC), San Jose, CA, Oct. 19–22, IEEE, pp. 1–7.
- [11] Bowen, J., Hausselle, J., and Gonzalez, R., 2018, “A Low-Cost Customizable Prosthetic Foot With Energy Return Capabilities,” *Prosthet. Orthot. Open J.*, **2**, pp. 1–5.
- [12] Hafner, B. J., 2005, “Clinical Prescription and Use of Prosthetic Foot and Ankle Mechanisms: A Review of the Literature,” *J. Prosthet. Orthot.*, **17**(Suppl.), pp. S5–S11.
- [13] Wezenberg, D., Cutti, A. G., Bruno, A., and Houdijk, H., 2014, “Differentiation Between Solid-Ankle Cushioned Heel and Energy Storage and Return Prosthetic Foot Based on Step-to-Step Transition Cost,” *J. Rehabil. Res. Dev.*, **51**(10), pp. 1579–1590.
- [14] Stevens, P. M., Rheinstein, J., and Wurdeman, S. R., 2018, “Prosthetic Foot Selection for Individuals With Lower-Limb Amputation: A Clinical Practice Guideline,” *J. Prosthet. Orthot.*, **30**(4), pp. 175–180.
- [15] International Organization for Standardization, 2016, ISO 10328:2016 – Prosthetics: Structural Testing of Lower-Limb Prostheses: Requirements and Test Methods.
- [16] International Organization for Standardization, 2006, ISO 22675:2006 – Prosthetics: Testing of Ankle-Foot Devices and Foot Units: Requirements and Test Methods.
- [17] Olesnavage, K. M., and Winter, A. G., 2018, “A Novel Framework for Quantitatively Connecting the Mechanical Design of Passive Prosthetic Feet to Lower Leg Trajectory,” *IEEE Trans. Neural Syst. Rehabil. Eng.*, **26**(8), pp. 1544–1555.
- [18] Olesnavage, K., Prost, V., Johnson, B., Major, M., and Winter, A. G., 2020, “Experimental Demonstration of the Lower Leg Trajectory Error Framework Using Physiological Data As Input,” *ASME J. Biomech. Eng.*, **143**(3), p. 031003.
- [19] Rouse, E. J., Hargrove, L. J., Perreault, E. J., and Kuiken, T. A., 2014, “Estimation of Human Ankle Impedance During the Stance Phase of Walking,” *IEEE Trans. Neural Syst. Rehabil. Eng.*, **22**(4), pp. 870–878.
- [20] Zhou, H., and Ting, K.-L., 2006, “Shape and Size Synthesis of Compliant Mechanisms Using Wide Curve Theory,” *ASME J. Mech. Des.*, **128**(3), pp. 551–558.
- [21] Zhu, B., Zhang, X., Zhang, H., Liang, J., Zang, H., Li, H., and Wang, R., 2020, “Design of Compliant Mechanisms Using Continuum Topology Optimization: A Review,” *Mech. Mach. Theory*, **143**, p. 103622.
- [22] McGuire, W., Gallagher, R. H., and Ziemian, R. D., 2014, *Matrix Structural Analysis*, 2nd ed, Wiley, Hoboken, NJ.
- [23] Mandell, J. F., McGarry, F. J., Huang, D. D., and Li, C. G., 1983, “Some Effects of Matrix and Interface Properties on the Fatigue of Short Fiber-Reinforced Thermoplastics,” *Polym. Compos.*, **4**(1), pp. 32–39.
- [24] Goldberg, D. E., 1989, *Genetic Algorithms in Search, Optimization, and Machine Learning*, Addison-Wesley, Boston, MA.
- [25] Winter, D. A., 2009, *Biomechanics and Motor Control of Human Movement*, 4th ed., John Wiley & Sons, Hoboken, NJ.
- [26] DESA, U., 2009, United Nations, Department of Economic and Social Affairs, Population Division, World Population Prospects 2019: Highlights.
- [27] Warder, H. H., Fairley, J. K., Coutts, J., Glisson, R. R., and Gall, K., 2018, “Examining the Viability of Carbon Fiber Reinforced Three-Dimensionally Printed Prosthetic Feet Created by Composite Filament Fabrication,” *Prosthet. Orthot. Int.*, **42**(6), pp. 644–651.
- [28] Montesano, J., Selezneva, M., Levesque, M., and Fawaz, Z., 2015, “Modeling Fatigue Damage Evolution in Polymer Matrix Composite Structures and Validation Using In-Situ Digital Image Correlation,” *Compos. Struct.*, **125**, pp. 354–361.
- [29] Smith, J. D., and Martin, P. E., 2013, “Effects of Prosthetic Mass Distribution on Metabolic Costs and Walking Symmetry,” *J. Appl. Biomech.*, **29**(3), pp. 317–328.
- [30] Bentham, J., Giwerzman, A., Sonestedt, E., Stocks, T., and NCD Risk Factor Collaboration, 2017, “Worldwide Trends in Body-Mass Index, Underweight, Overweight, and Obesity From 1975 to 2016: A Pooled Analysis of 2416 Population-Based Measurement Studies in 128.9 Million Children, Adolescents, and Adults,” *Lancet*, **390**(10113), pp. 2627–2642.
- [31] Eng, J. J., and Winter, D. A., 1995, “Kinetic Analysis of the Lower Limbs During Walking: What Information Can Be Gained From a Three-dimensional Model?,” *J. Biomech.*, **28**(6), pp. 753–758.
- [32] Ernst, M., Altenburg, B., and Schmalz, T., 2020, “Characterizing adaptations of prosthetic feet in the frontal plane,” *Prosthet. Orthot. Int.*, **44**(4), pp. 225–233.
- [33] Fukuchi, C. A., Fukuchi, R. K., and Duarte, M., 2018, “A public dataset of overground and treadmill walking kinematics and kinetics in healthy individuals,” *PeerJ*, **6**, p. e4640.